Geophysical Research Letters

RESEARCH LETTER
10.1029/2019GL086383

The Far Ultraviolet Signatures of Conjugate Photoelectrons Seen by the Special Sensor Ultraviolet Spectrographic Imager

Hyosub Kil[1], Robert K. Schaefer[1], Larry J. Paxton[1], and Geonhwa Jee[2]

[1]The Johns Hopkins University Applied Physics Laboratory, Laurel, MD, USA, [2]Korea Polar Research Institute, Incheon, South Korea

Key Points:

- Global morphology of conjugate photoelectrons is derived for the first time using the measurements of far ultraviolet emissions by SSUSI
- Anomalous oxygen atom 130.4 nm emissions appear at night in the winter hemisphere at the longitudes close to the magnetic poles
- Anomalous emission morphology is explained by the magnetic field configuration and solar zenith angle

Correspondence to:
H. Kil,
hyosub.kil@jhuapl.edu

Citation:
Kil, H., Schaefer, R. K., Paxton, L. J., & Jee, G. (2020). The far ultraviolet signatures of conjugate photoelectrons seen by the Special Sensor Ultraviolet Spectrographic Imager. *Geophysical Research Letters*, *47*, e2019GL086383. https://doi.org/10.1029/2019GL086383

Received 22 NOV 2019
Accepted 20 DEC 2019
Accepted article online 3 JAN 2020

Abstract This study investigates the origin of anomalous far ultraviolet emissions observed at night at the subauroral region by the Special Sensor Ultraviolet Spectrographic Imager on board the Defense Meteorological Satellite System-F16 satellite. The global distribution of the anomalous emission is derived using the measurements of the oxygen atom 130.4-nm emission in 2017. Our results show the extension of the anomalous emission from high latitudes to middle latitudes in the Northern American-Atlantic sector during the December solstice and in the Southern Australia-New Zealand sector during the June solstice. These observations indicate that the anomalous emission occurs in the winter hemisphere and is pronounced at locations close to the magnetic poles. The good agreement between the morphology of the anomalous emission and the predicted distribution of conjugate photoelectrons leads to the conclusion that the anomalous emissions are the signatures of conjugate photoelectrons.

Plain Language Summary Conjugate photoelectrons are photoelectrons that originate from the magnetic conjugate locations in the sunlit hemisphere. Their existence is manifested by the observations of anomalous airglow and electron temperature enhancements at night. However, previous observations of conjugate photoelectrons were mostly confined to twilight at limited longitudes, and therefore, their global behavior has not yet been identified. This study derives the global morphology of conjugate photoelectrons using the measurements of far ultraviolet emissions by the Special Sensor Ultraviolet Spectrographic Imager on board the Defense Meteorological Satellite Program-F16 satellite in 2017. Anomalous emissions of oxygen atom 130.4 nm are detected at night in the winter hemisphere preferentially at locations close to magnetic poles. These characteristics are consistent with the predicted distribution of conjugate photoelectrons. Our results demonstrate that far ultraviolet observations from space are valuable resources for the study of conjugate photoelectrons.

1. Introduction

Photoionization of neutral particles on the sunlit side of the atmosphere produces suprathermal electrons whose energy is greater than that of ambient, thermalized electrons. These suprathermal electrons on the sunlit side flow into the nightside along the magnetic field lines and lose their energy through collisions with neutral particles and plasma at the local region. “Conjugate photoelectrons” represent those suprathermal electrons that have traveled from the magnetic conjugate locations. Conjugate photoelectrons are manifested by the observations of electron temperature enhancement at predawn by radars (Carlson, 1966; Evans, 1967; Evans & Gastman, 1970) and satellites (Kakinami et al., 2010; Oyama et al., 1996), observations of airglow at visual (Bennett, 1969; Carlson & Suzuki, 1974; Christensen, 1975; Duboin et al., 1968; Shepherd et al., 2014) and far ultraviolet (FUV) (Buckley & Moos, 1971; Meier, 1971) wavelengths, measurements of photoelectron fluxes by satellites (Peterson et al., 1977, 2009; Richards & Peterson, 2008), and simultaneous in situ rocket measurements of airglow, electron density and temperature, and photoelectron flux (Shepherd et al., 1978). A variety of methods have been used to model the generation, transport, and impact of photoelectrons (Varney et al., 2012, and references therein).

Ground-based optical observations of oxygen atom (OI) lines at visible wavelengths at twilight were a popular method used in 1960s and 1970s to study conjugate photoelectrons. However, the extraction of the direct photoelectron impact component from the emissions at visible wavelengths is not straightforward because photochemical reactions as well as photoelectrons contribute to the emission (Christensen, 1975). The

interpretation of the FUV emissions is less complicated because conjugate photoelectrons dominate the production of the FUV airglow when the auroral particle precipitation and direct photoionization are absent. The FUV signatures of conjugate photoelectrons in the observations of OGO-4 satellite (Meier, 1971) and rocket probes (Buckley & Moos, 1971) indicate that a significant number of conjugate photoelectrons carry energy above 10 eV. While the radiative recombination of oxygen ions in the ionosphere is also an important source of FUV emissions at night in low latitudes, this emission is much weaker than that produced by conjugate photoelectrons in middle latitudes during magnetically quiet periods. Compared with the emissions produced by energetic particle precipitations in the auroral region, the emissions produced by conjugate photoelectrons have a tell-tale spectral signature as they consist of just the oxygen 130.4- and 135.6-nm emissions and no N_2 Lyman-Birge-Hopfield (LBH) emissions. As the references cited above show, there has been relatively little work on the subject of conjugate photoelectrons recently.

The observations of atmospheric FUV emissions by the Special Sensor Ultraviolet Spectrographic Imager (SSUSI) on board Defense Meteorological Satellite Program (DMSP) and the Global Ultraviolet Imager on board the Thermosphere Ionosphere Mesosphere Energetics and Dynamics satellites provide a unique resource for the study of the global behavior of conjugate photoelectrons. However, these data have not yet been explored for this purpose. This study reports anomalous FUV emissions in DMSP-F16/SSUSI observations that are suspected to be the signatures of conjugate photoelectrons. We use the terminology "anomalous" in this paper because the emissions that we report are not explained by the effects of direct photoionization or high energy particle precipitation. The global distribution of the anomalous FUV emissions is derived using the measurements of the OI 130.4 nm line by DMSP-F16/SSUSI in 2017. We assess the association of the anomalous OI 130.4-nm emissions with conjugate photoelectrons by examining their dependence on the geomagnetic field configuration and solar zenith angle (SZA).

2. Data Description

DMSP F16 was launched on 18 October 2003. It has a circular sun-synchronous orbit at an altitude of 840 km with an orbital inclination of 98°. Currently, the local solar times (LSTs) of the ascending and descending orbits of F16 at the equator are 15.5 and 3.5 hr, respectively. The SSUSI instrument on board DMSP F16, F17, F18, and F19 satellites is a FUV imaging spectrograph and provides disk- and limb- scan images. Due to data rate constraints on the spacecraft side, the spectral images are combined, for downlink in imaging mode, into five wavelength intervals: HI 121.6 nm, OI 130.4 nm, OI 135.6 nm, N_2 LBH from 140.0 to 150.0 nm (LBH Short) and from 165.0 to 180 nm (LBH Long) (Paxton et al., 1992, 2002, 2017, 2018); the entire spectrum can be downlinked if the scan mirror is not in motion, again, due to data rate constraints.

The instrument slit aperture is aligned with the orbital along track direction. In imaging mode, the slit looks at a mirror that is scanned across the Earth, in a "whisk broom" imaging mode; in spectrograph mode the scan mirror is fixed in a particular direction and the entire available spectrum is downlinked. When F16's routine imaging mode operations were halted on 23 August 2016, the scan mirror was positioned to look 47° off nadir, away from the sun. In spectrograph mode, the spatial information along the image of the slit is recorded as eight along track pixels. The analysis reported in this paper used the spectrographic level 1C products (called Sensor Data Records for SSUSI) in which these individual pixels are averaged together in 25 km along-track bins. The OI 130.4 and OI 135.6 nm lines in these products are fully calibrated and background subtracted using the same methods as in their imaging mode counterparts. These data products are available at the SSUSI (https://ssusi.jhuapl.edu) website.

To use the data, we must ensure that our key observations are not contaminated by detector particle noise, which occurs in the South Atlantic Anomaly (SAA) and the subauroral zone (Schaefer et al., 2016). The SAA, centered near 300°E longitude and 25°S latitude, is the region where the magnetic field is weak and energetic particles from the inner radiation belt precipitate. The SAA has already been removed from the SSUSI Sensor Data Record data. The subauroral emission is due to quasi-trapped MeV electrons (e.g., Tu et al., 2010). The noise from quasi-trapped electrons occurs after geomagnetic storms and fades after several days depending on the details of the storm. This noise is considerably more difficult to remove in an automated fashion from the SSUSI data. However, the noise from this emission occurs at magnetic latitudes close to the aurora and at much higher latitudes than the anomalous emissions studied here, so it does not affect our conjugate emission morphology.

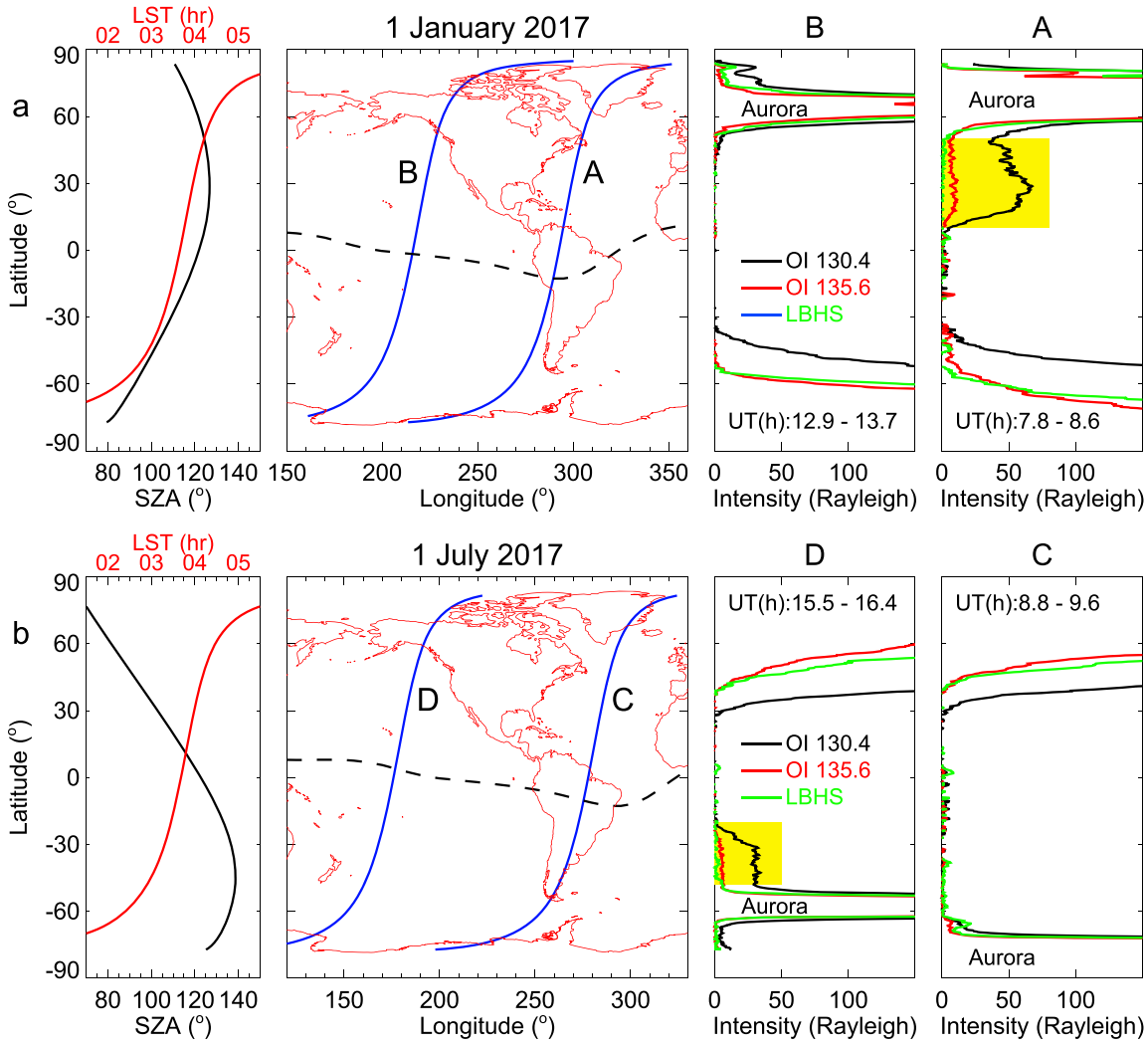

Figure 1. Examples of F16/SSUSI observations on (a) 1 January 2017 and (b) 1 July 2017. From left to right, solar zenith angle (black) and solar local time (red), ground tracks of SSUSI field of view at the pierce point of 350 km altitude, and observations of OI 130.4, OI 135.6, and LBHS lines are shown. The anomalous OI emissions on orbit A and D are indicated by yellow shadings. The black dashed line in the map is the magnetic equator.

3. Observational Results

The observations in Figure 1 show the typical anomalous FUV emission features in F16/SSUSI data in two seasons: (a) 1 January 2017 and (b) July 1 2017. From left to right, SZA and LST, F16 orbits, and FUV emission data at the pierce point of the field of view at an altitude of 350 km are shown. The OI 130.4, OI 135.6, and LBH Short (LBHS) emission data are distinguished by black, red, and blue, respectively. The observations were made after midnight. The Kp indices of 3-hr intervals from 0 to 24 UT were 3^{+}, 4^{-}, 3^{-}, 2^{+}, 2^{+}, 3^{0}, 2^{0}, and 2^{-} on 1 January and 2^{-}, 3^{+}, 3^{-}, 2^{-}, 3^{-}, 3^{0}, 3^{+}, and 2^{0} on 1 July. The locations of aurora are distinguished by strong emissions in the winter hemisphere. In the summer hemisphere, however, the steep boundaries of the strong FUV emissions are associated with the movement of the satellite orbit into the sunlit. The anomalous OI emissions are indicated by yellow shadings. These features are anomalous because they occur at the subauroral region (outside the region where energetic particle precipitation occurs) on the nightside (no photoionization). Note the absence of the anomalous emission feature in the LBHS emission; this would be expected for "soft" conjugate photoelectrons as they will be stopped at high altitudes where the predominant constituent is O. From the summary images of SSUSI data at the SSSUI website (https://ssusi.jhuapl.edu/), we have identified the recurrence of the anomalous FUV emissions in OI lines at specific longitudes in the winter hemisphere.

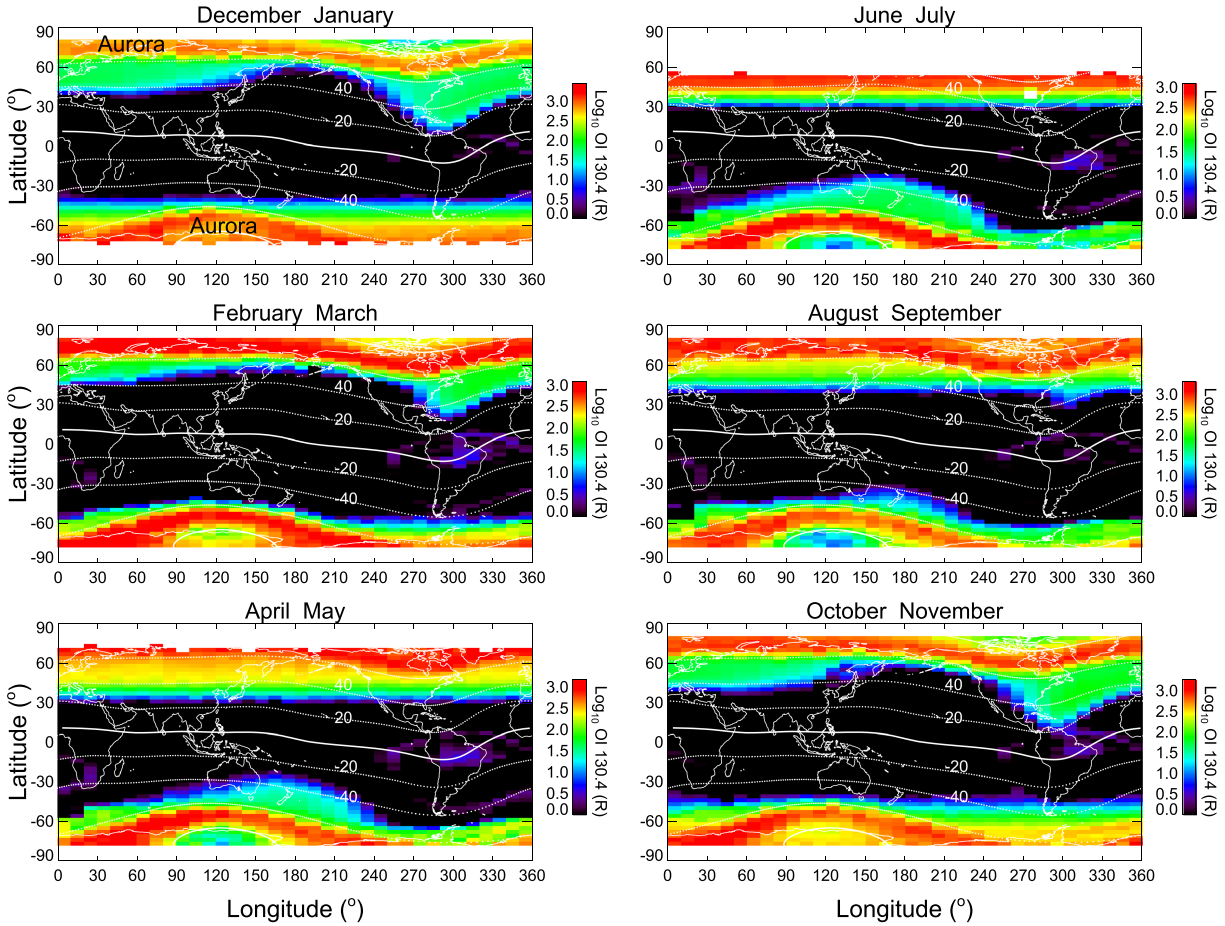

Figure 2. OI 130.4-nm intensity maps in six periods of a year. The maps are produced using the F16/SSUSI data in 2017 with the threshold SZA > 90°. The white lines indicate magnetic latitudes.

The global behavior of the anomalous OI emission is investigated using the maps of OI 130.4 nm intensity for six periods of a year. Because the morphology of the anomalous emission seen by the OI 135.6 nm emission is the same as that seen by the OI 130.4 nm emission except for the emission intensity, we present only the maps of OI 130.4 nm in Figure 2. The mean intensities on 10° × 3° longitude and latitude bins are obtained using the F16/SSUSI data in 2017 for the threshold SZA > 90°. The white dotted lines are the magnetic latitudes. The locations of aurora, as indicated on the map in December and January, can be identified by bright curved bands in high latitudes. Horizontal straight emission layers in the summer hemisphere are produced by the solar illumination of the atmosphere even for SZA greater than 90°. Recall that all of the DMSP SSUSIs are in orbits with a fixed LST; for any given day, the solar zenith angle at a particular latitude is constant. Thus, within the limitations of the color bar, the intensity of the dayglow appears as a constant at a given latitude.

We note the emissions at subauroral region that show a strong seasonal and longitudinal dependence. As we have already described, we call these features "anomalous emissions." In December and January, the anomalous emission is pronounced in the American-Atlantic sector (240°–330°E) in the Northern Hemisphere. This feature extends to 20°N magnetic latitude at 290°E longitude. The anomalous emission is also noticeable in 0°–120°E longitude in the Northern Hemisphere. These anomalous emissions retreat to higher latitudes in February and March, are invisible in April–September, and reappear in October–November. In the Southern Hemisphere, the anomalous emission is pronounced at 100°–240°E longitude in June and July. This feature is weakened in April and May and August and September and is invisible in October–January. Thus, the anomalous emissions in both Northern and Southern Hemispheres are phenomena pronounced in the winter and in the longitudes close to the longitudes of magnetic poles.

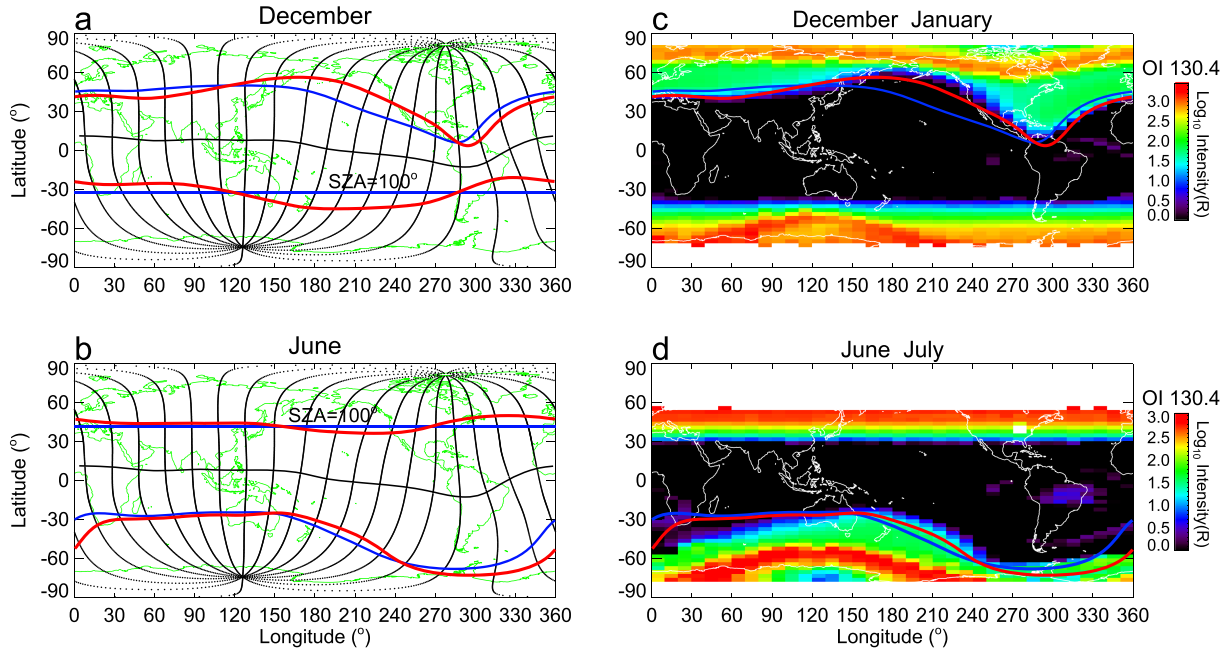

Figure 3. (a and b) Earth's magnetic field configuration and magnetic conjugacy on 22 December and 22 June. The blue and red lines in the summer hemisphere indicate the locations of 100° SZA calculated using two different methods. Their magnetic conjugate locations are shown by the same color. See the text for the details of the blue and red lines. (c and d) SSUSI OI 130.4 maps in December and January and June and July with the conjugate SZA lines shown in Figures 3a and 3b.

4. Conjugate Photoelectron Distribution

We can think about three potential sources of the anomalous OI emissions at night: particle precipitation, radiative recombination of oxygen ions in the ionosphere, and conjugate photoelectrons. The radiative recombination of oxygen ions is an important source of the OI emissions at night in the region where the oxygen ion density is significant. However, the observed anomalous OI emissions are much stronger than the emissions produced by the radiative recombination at midlatitudes. If the anomalous OI emissions are related to the radiative recombination, the ionospheric plasma density at night would show a morphology similar to that of the OI emissions. However, the anomalous OI emission feature does not correlate with any observations of enhanced plasma density (e.g., Lee et al., 2018).

The dependence of the locations of the anomalous OI emissions on the locations of the magnetic poles and magnetic declination is a strong indication of the control of the anomalous OI emissions by the magnetic field configuration. Because the interhemispheric flow of conjugate photoelectrons is controlled by the geomagnetic field configuration, conjugate photoelectrons are plausible sources of the anomalous OI emissions. We infer the interhemispheric flow of photoelectrons using the geomagnetic field configuration and SZA at the points of observation.

The black dots in Figures 3a and 3b show the geomagnetic field lines derived using the Altitude Adjusted Corrected GeoMagnetic model (Baker & Wing, 1989) in the geographic longitude and latitude coordinates. The OI 130.4 nm maps for the December and June solstices are shown in Figures 3c and 3d to compare with the predicted distribution of conjugate photoelectrons. We first explain the blue lines in Figure 3a. The straight blue line in the Southern (summer) Hemisphere indicates 100° SZA at 4.0 hr LST. The blue line in the Northern (winter) Hemisphere is its magnetic conjugate location. 100° SZA corresponds to the sunset time near an altitude of 100 km. This is a conservative boundary; sunset effectively occurs at earlier times (lower SZA) for the wavelengths of sunlight that create ionization due to the wavelength dependent attenuation of sunlight along the line of sight from the Sun to the point in the atmosphere under consideration. Because photoelectrons exist poleward of the blue line in the Southern Hemisphere and these photoelectrons can travel to the Northern Hemisphere along the magnetic field lines, the blue line in the Northern Hemisphere represents the latitudinal boundary of conjugate photoelectrons. We have chosen 4.0 hr LST

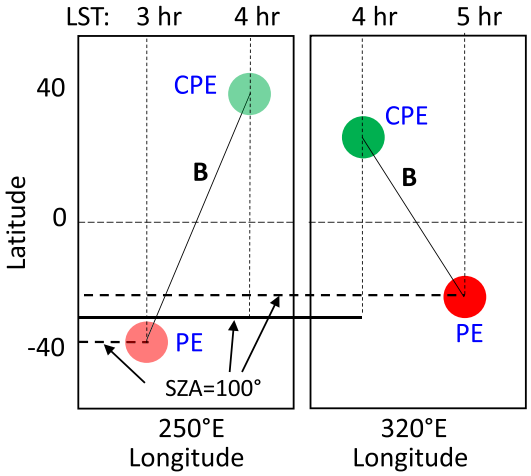

Figure 4. Schematic illustration of the origin of conjugate photoelectrons in the regions of different magnetic declinations during the December solstice. Green shadings represent the locations of conjugate photoelectrons (CPE) or anomalous emissions caused by photoelectrons (PE) from the locations of red shadings. B is the magnetic field line. The brightness of green and red shadings at the two longitudes are different to emphasize the difference of the characteristics of CPE that originate from different latitudes and LSTs. The diagram also illustrates the variation of the latitude of 100° SZA with LST.

for the conjugate calculation to match the LST of the SSUSI observation in the Northern Hemisphere (see left panel in Figure 1a). The same method is used for the blue lines in Figure 3b. In the June solstice, the latitude of the 100° SZA and its conjugate locations are calculated for 3.25 hr LST to match the LST of the SSUSI observation in the Southern Hemisphere (see left panel in Figure 1b). The blue lines in the winter hemisphere are shown in Figures 3c and 3d. The large-scale morphology of the anomalous emission is represented by the blue lines, but significant deviations also exist.

The blue lines assume that photoelectrons are produced at the same LST (4 hr in the December solstice and 3.25 hr in the June solstice) at all longitudes in the summer hemisphere and are responsible for the conjugate photoelectrons at the same LST in the winter hemisphere. This assumption is reasonably accurate for the longitudes where the magnetic declination is zero. At the longitudes where the magnetic declination is nonzero, however, conjugate photoelectrons originate from the regions of different LSTs. We explain the situations around 250°E (positive magnetic declination) and 320°E (negative magnetic declination) longitudes during the December solstice using the diagram in Figure 4. Green shadings assume the observations of the anomalous emissions (conjugate photoelectrons) at 4 hr LST in the Northern Hemisphere during the December solstice, and red shadings are the origins of the conjugate photoelectrons. The diagram indicates the difference of the LSTs of the field lines at the green and red shadings. Around 250°E, the anomalous emission at 4 hr LST in the Northern Hemisphere is produced by the photoelectrons created at an earlier time (3 hr LST) in the Southern Hemisphere. Then, we have to find the location of the 100° SZA at 3.0 hr LST instead of at 4.0 hr LST in the Southern (summer) Hemisphere. Because the latitude of 100° SZA is the highest at midnight and moves to lower latitudes as a function of time relative to midnight, the location of 100° SZA at 3.0 hr LST is at a higher latitude than that at 4.0 hr LST. The opposite situation occurs at 320°E; the photoelectrons produced at 5.0 hr LST in the Southern Hemisphere are responsible for the anomalous emission detected at 4.0 hr LST in the Northern Hemisphere. The location of 100° SZA at 5.0 hr LST is at a lower latitude than that at 4.0 hr LST. The diagram schematically illustrates the variation of the latitude of 100° SZA for different LSTs. In Figure 3a, the red line in the Southern Hemisphere shows the corrected 100° SZA after taking care of the magnetic declination effect. For this correction, we have identified the magnetic field line at each geographic longitude at 4.0 hr LST at 40°N geographic latitude. Then, the SZA is calculated along the field line, and the location (geographic longitude and latitude) when the SZA becomes 100° in the Southern Hemisphere is determined. We have chosen 40°N as the reference location of the anomalous emission, but our result is not sensitive to the selection of the reference latitude. The red lines in Figure 3b are obtained using the same method for 40°S reference latitude and 3.25 hr LST. Depending on the magnetic field configuration, the locations of 100° SZA and its conjugate locations shift to higher or lower latitudes relative to the blue line. This variation is consistent with our explanation of the dependence of the latitude of 100° SZA on the magnetic declination. In Figures 3c and 3d, the morphology of the anomalous emission is represented better after taking into account the magnetic declination effect (red lines).

The intensity of the anomalous emission is determined by the characteristics of conjugate photoelectrons (energy and flux) and neutral gases (density and composition). Because these characteristics vary with geophysical and geographic parameters, the intensity of the anomalous emission also varies with those parameters. Although numerical simulations are required to understand the variability of the emission intensity, we can infer the source of some variations by considering the magnetic declination effect. By focusing on the emission intensity near the red line in Figure 3c, we can identify the weaker emission intensity around 250°E longitude compared with that around 320°E longitude. As the diagram in Figure 4 shows, the conjugate photoelectrons around 250°E come from at higher latitude and earlier LST (closer to

midnight) relative to those around 320°E. The production rate of photoelectrons would vary with latitude and LST, and therefore, the emissions produced by those photoelectrons originated from different latitudes and LSTs would also be different. Poleward of the red line in Figure 3d, the emission intensity around 30°E is weaker compared to that around 210°E. Considering the geomagnetic field configuration in Figure 3b, conjugate photoelectrons around 30°E originate from higher latitudes and earlier LST (closer to midnight) relative to those around 210°E. Thus, the emission is weaker in the longitudes where conjugate photoelectrons originate from higher latitudes and closer to midnight in both seasons.

5. Conclusions

Anomalous OI 130.4 and 135.6 nm emissions are identified on the nightside at subauroral locations from the DMSP-F16/SSUSI observations. They occur in the winter hemisphere and are pronounced at the longitudes close to the magnetic poles. These characteristics are not explained by direct photoionization, particle precipitation, or radiative recombination of oxygen ions in the ionosphere. Excluding those sources, conjugate photoelectrons that travel from the sunlit side in the summer hemisphere are the only plausible sources of the anomalous emissions. This interpretation is supported by the good agreement between the morphology of anomalous emissions and the predicted distribution of conjugate photoelectrons which is determined by the geomagnetic field configuration and SZA.

This paper demonstrates that the observations of FUV emissions from space are valuable resources for the study of conjugate photoelectrons. The FUV emissions produced by conjugate photoelectrons are the consequence of the production of photoelectrons in the sunlit side, their interhemispheric transport, and their impact on the conjugate atmosphere. These processes are sensitive to the solar flux, the density, velocity, composition, and temperature of neutral and charged particles. The behavior of conjugate photoelectrons during magnetically disturbed periods is expected to be different from that during magnetically quiet periods because of the changes in the ionospheric and thermospheric conditions. The interhemispheric photoelectron flow through the magnetosphere and thermosphere will also be affected by geomagnetic disturbances. The FUV observations by SSUSI and Global Ultraviolet Imager can be used for the study of the behavior of conjugate photoelectrons under different geophysical conditions and the validation of the characteristics of conjugate photoelectrons in photoelectron models.

Acknowledgments
The work at JHU/APL was supported by DMSP SSUSI program, MURI FA9559-16-1-0364 and KOPRI PE20100. All SSUSI data used in this paper are available from https://ssusi.jhuapl.edu website.

References

Baker, K. B., & Wing, S. (1989). A new magnetic coordinate system for conjugate studies at high latitudes. *Journal of Geophysical Research*, *94*(a7). https://doi.org/10.1029/JA094iA07p09139

Bennett, R. T. (1969). Latitude dependence of 6300A (OI) twilight airglow enhancement. *Journal of Geophysical Research*, *74*(1). https://doi.org/10.1029/JA074i001p00381

Buckley, J. L., & Moos, H. W. (1971). Vacuum ultraviolet spectra of the late twilight airglow. *Journal of Geophysical Research*, *76*(34). https://doi.org/10.1029/JA076i034p08378

Carlson, H. C. (1966). Ionospheric heating by magnetic conjugate-point photoelectrons. *Journal of Geophysical Research*, *71*(1). https://doi.org/10.1029/JZ071i001p00195

Carlson, R. W., & Suzuki, K. (1974). Observation of O^+ ($^2P_o - {}^2D_o$) λ 7319 Å emission in the twilight and night airglow. *Nature*, *248*, 400–401 . https://doi.org/10.1038_248400a0

Christensen, A. B. (1975). Observations of OI 7774 emission excited by conjugate photoelectrons. *Planetary and Space Science*, *23*, 831–842. https://doi.org/10.1016/0032-0633(75)90020-3

Duboin, M.-L., Lejeune, G., Petit, M., & Weill, G. (1968). Excitation of oxygen ion lines and ionospheric heating by conjugate photoelectrons. *Journal of Atmospheric and Terrestrial Physics*, *30*, 299–304. https://doi.org/10.1016/0021-9196(68)90084-6

Evans, J. V. (1967). Midlatitude electron and ion temperatures at sunspot minimum. *Planetary and Space Science*, *15*, 1557–1570. https://doi.org/10.1016/0032-0633(67)90089-X

Evans, J. V., & Gastman, I. J. (1970). Detection of conjugate photoelectrons at Millstone Hill. *Journal of Geophysical Research*, *75*(2). https://doi.org/10.1029/JA075i004p00807

Kakinami, Y., Balan, N., Liu, J. Y., & Oyama, K.-I. (2010). Predawn ionospheric heating observed by Hinotori satellite. *Journal of Geophysical Research*, *115*, A01304. https://doi.org/10.1029/2009JA014334

Lee, W. K., Kil, H., & Paxton, L. J. (2018). Tropical ionization trough seen by Swarm-A satellite. *Geophysical Research Letters*, *45*, 12,135–12,141. https://doi.org/10.1029/2018GL080286

Meier, R. R. (1971). Observations of conjugate excitation of the O I 1304-A airglow. *Journal of Geophysical Research*, *76*(1). https://doi.org/10.1029/JA076i001p00242

Oyama, K.-I., Balan, N., Watanabe, S., Takahashi, T., Isoda, F., Bailey, G. J., & Oya, H. (1996). Morning overshoot of Te enhanced by downward plasma drift in the equatorial topside ionosphere. *Journal of Geomagnetism and Geoelectricity*, 48. https://doi.org/10.5636/jgg.48.959

Paxton, L. J., Meng, C.-I., Fountain, G. H., Ogorzalek, B. S., Darlington, E. H., Gary, S. A., et al. (1992). SSUSI: Horizon-to-horizon and limb-viewing spectrographic imager for remote sensing of environmental parameters. *Proceedings of SPIE*, *1764*, 161–176. https://doi.org/10.1117/12.140846

Paxton, L. J., Morrison, D., Zhang, Y., Kil, H., Wolven, B., Ogorzalek, B. S. et al. (2002). Validation of remote sensing products produced by the Special Sensor Ultraviolet Scanning Imager (SSUSI): A far UV imaging spectrograph on DMSP F-16. Proc. SPIE, *4485*, Optical Spectroscopic Techniques, Remote Sensing, and Instrumentation for Atmospheric and Space Research IV. https://doi.org/10.1117/12.454268

Paxton, L. J., Schaefer, R., Zhang, Y., & Kil, H. (2017). Far ultraviolet instrument technology. *Journal of Geophysical Research: Space Physics*, *122*, 2706–2733. https://doi.org/10.1002/2016JA023578

Paxton, L. J., Schaefer, R. K., Zhang, Y., Kil, H., & Hicks, J. E. (2018). SSUSI and SSUSI-Lite: Providing space situational awareness and support for over 25 years. *Johns Hopkins APL Technical Digest*, *34*(3), 388–400.

Peterson, W. K., Doering, J. P., Potemra, T. A., McEntire, R. W., & Bostrom, C. O. (1977). Conjugate photoelectron fluxes observed on Atmosphere Explorer C. *Geophysical Research Letters*, *4*, 109. https://doi.org/10.1029/GL004i003p00109

Peterson, W. K., Stavros, E. N., Richards, P. G., Chamberlin, P. C., Woods, T. N., Bailey, S. M., & Solomon, S. C. (2009). Photoelectrons as a tool to evaluate spectral variations in solar EUV irradiance over solar cycle timescales. *Journal of Geophysical Research*, *114*, A10304. https://doi.org/10.1029/2009JA014362

Richards, P. G., & Peterson, W. K. (2008). Measured and modeled backscatter of ionospheric photoelectron fluxes. *Journal of Geophysical Research*, *113*, A08321. https://doi.org/10.1029/2008JA013092

Schaefer, R. K., Paxton, L. J., Selby, C., Ogorzalek, B. S., Romeo, G., Wolven, B. C., & Hsieh, S.-Y. (2016). Observation and modeling of the South Atlantic Anomaly in low Earth orbit using photometric instrument data. *Space Weather*, *14*, 330–342. https://doi.org/10.1002/2016SW001371

Shepherd, G. G., Cho, Y.-M., Fomichev, V. I., & Martynenko, O. V. (2014). Characteristics of the O^{+}(2P–2D) 732.0 and 733.0 nm airglow emissions observed with WINDII and simulated with the C-IAM. *Geophysical Research Letters*, *41*, 5354–5360. https://doi.org/10.1002/2014GL060840

Shepherd, G. G., Pieau, J. F., Ogawa, T., Tohmatsu, T., Oyama, K., & Watanabe, Y. (1978). Direct measurement of conjugate photoelectrons and predawn 630 nm airglow. *Planetary and Space Science*, *26*, 221–217. https://doi.org/10.1016/0032-0633(78)90086-7

Tu, W., Selesnick, R., Li, X., & Looper, M. (2010). Quantification of the precipitation loss of radiation belt electrons observed by SAMPEX. *Journal of Geophysical Research*, *115*, A07210. https://doi.org/10.1029/2009JA014949

Varney, R. H., Swartz, W. E., Hysell, D. L., & Huba, J. D. (2012). SAMI2-PE: A model of the ionosphere including multistream interhemispheric photoelectron transport. *Journal of Geophysical Research*, *117*, A06322. https://doi.org/10.1029/2011JA017280